

**DEVELOPMENT AND CHARACTERIZATION
OF POLYMER GEL DOSIMETER DOPED WITH
GOLD NANOPARTICLES**

MUHD HAZWAN HAKIM BIN HISHAM

UNIVERSITI SAINS MALAYSIA

2023

**DEVELOPMENT AND CHARACTERIZATION
OF POLYMER GEL DOSIMETER DOPED WITH
GOLD NANOPARTICLES**

by

MUHD HAZWAN HAKIM BIN HISHAM

**Thesis submitted in fulfilment of the requirements
for the Degree of
Doctor of Philosophy**

August 2023

ACKNOWLEDGEMENT

First and foremost, I am grateful to Allah the Almighty. I am able to finish this thesis with willing and his mercy. He grants me health, patience and strength throughout this hard journey. I am blessed by Him with a very supportive circle of people that made me move forward and overcame multiple obstacles.

I would like to thank Assc. Prof. Dr. Azhar Abdul Rahman, my supervisor for 7 years. He layout the foundation for me guide me throughout my PhD. journey. His patience after a few postponements from me is something I am grateful for. There were no difficult times in dealing with him because he has always been a cooperative and understanding supervisor.

Special thanks to Assc. Prof. Dr. Iskandar Shahrim Mustafa and Dr. Nik Nur Ashikin of School of Physics, USM where they are my unofficial advisor anytime I was stuck in my research. I would like to express my gratitude towards School of Physics, USM for letting me use the facilities especially in the Biophysics and Medical Physics laboratory. My thankfulness is extended towards Advanced Medical and Dental Institute (AMDI), USM for the cooperation giving the permission to use MRI unit and Pantai Hospital, Bayan Baru for the use of LINAC.

On my personal note, firstly I am hugely indebted to my parents who always be my biggest supporter in my study. They have helped me financially, emotionally and mentally in ensuring I completed my study. To the person who I strongly depend on my down time, my wife, words can never describe my gratefulness by having you by my side. These humble words are not enough to give my appreciation to all.

TABLE OF CONTENTS

ACKNOWLEDGEMENT	ii
TABLE OF CONTENTS	iii
LIST OF TABLES	vii
LIST OF FIGURES	ix
LIST OF ABBREVIATIONS	xiv
CHAPTER 1 INTRODUCTION	1
1.1 Background	1
1.2 Problem Statement	3
1.3 Objectives	4
1.4 Scope of study	4
1.5 Thesis outline.....	5
CHAPTER 2 THEORY AND LITERATURE REVIEW	6
2.1 Discovery of x-ray	6
2.2 Production of x-ray	6
2.3 Types of x-rays	7
2.3.1 Bremsstrahlung	7
2.3.2 Characteristic x-ray	8
2.4 Interaction of photons with matter	10
2.4.1 Rayleigh scattering.....	10
2.4.2 Photoelectric effect	11
2.4.3 Compton Effect.....	12
2.4.4 Pair Production.....	13
2.5 The Attenuation of X-ray	14

2.5.1	Linear Attenuation Coefficient	14
2.6	Linear Accelerator (LINAC).....	15
2.7	UV-Visible spectrophotometer	15
2.7.1	Effect of concentration and container shape on absorbance	17
2.7.2	Beer-Lambert Law	17
2.8	Polymer gel dosimetry	18
2.8.1	Fricke gel dosimeters	18
2.8.2	Acrylic based polymer gel dosimeters	20
2.8.3	Normoxic polymer gel	21
2.8.4	Ascorbic acid as anti-oxidant.....	23
2.8.5	Polymerization of Polymer Gel	24
2.9	Dosimetry and Radiation	27
2.10	Three-dimensional (3D) dosimeter	27
2.11	Magnetic Resonance Imaging (MRI) of polymer gels.....	29
2.12	Dose enhancement in polymer gel	31
2.13	Gold Nanoparticles (AuNPs) as Dose Enhancer.....	32
2.14	Absorbed dose.....	33
CHAPTER 3 MATERIALS & METHODS		35
3.1	Materials	35
3.2	Samples preparation.....	37
3.2.2	Post development	39
3.2.3	Irradiation of samples	39
3.3	Tissue equivalent material as phantom	39
3.4	Data collection and analysis.....	41
CHAPTER 4 RESULT & DISCUSSION		42
4.1	Analysis of HEMA polymerisation using UV-Vis spectrophotometer	42

4.1.1	AuNP 15nm	43
4.1.2	AuNP 20 nm	44
4.1.3	AuNP 40 nm	46
4.1.4	AuNP 50 nm	47
4.1.5	AuNP 80 nm	49
4.1.6	LINAC energy of 10 Gy	51
4.1.7	LINAC energy 20 Gy.....	51
4.1.8	LINAC energy 30 Gy.....	52
4.1.9	LINAC energy 40 Gy.....	53
4.1.10	LINAC energy 50 Gy.....	55
4.2	Analysis of HEMA polymerisation using MRI	56
4.2.1	HEMA irradiated with LINAC	56
4.2.2	HEMA irradiated with diagnostic x-ray.....	58
4.2.2.(a)	Gold nanoparticle (AuNp) size 15 nm	58
4.2.2.(b)	AuNp size 20 nm	60
4.2.2.(c)	AuNp size 50 nm	62
4.2.2.(d)	AuNp size 80 nm	64
4.2.2.(e)	HEMA 5%	66
4.2.2.(f)	HEMA 6%	68
4.2.2.(g)	HEMA 7%	70
4.2.2.(h)	HEMA 8%	72
4.2.2.(i)	HEMA 9%	74
4.3	Analysis of HEA using uv-vis spectrophotometer.....	76
4.3.1	Samples with no AuNPs	77
4.3.2	15 nm AuNP	79
4.3.3	20 nm AuNP	81

4.3.4	Samples doped with 50 nm AuNP	83
4.4	The effect of HEA concentration at several size of AuNPs.....	85
4.4.1	No AuNP.....	85
4.4.2	AuNP 15 nm	87
4.4.3	AuNP 20 nm	89
4.4.4	AuNP 50 nm	91
4.4.5	AuNP 80 nm	93
4.4.6	Effect of AuNps size	95
CHAPTER 5 CONCLUSION AND FUTURE WORK.....		98
5.1	Conclusion	98
5.2	Future work.....	100
REFERENCES.....		101

LIST OF TABLES

		Page
Table 2.1	Principal characteristic x-ray energies for Tungsten (Radiological Health Handbook Revised Edition, 1970)	10
Table 2.2	Several polymer gel dosimeters manufactured under normoxic condition	22
Table 3.1	Element composition with their respective concentration for HEMA polymer gel.....	38
Table 3.2	Element composition with their respective concentration for HEA polymer gel.....	38
Table 4.1	Dose sensitivity and correlation coefficient for different size AuNPs for HEMA irradiated with LINAC.....	57
Table 4.2	Dose sensitivity and correlation coefficient for different concentration of HEMA doped with 15 nm AuNP irradiated with diagnostic x-ray unit.....	60
Table 4.3	Dose sensitivity and correlation coefficient for different concentration of HEMA doped with 20 nm AuNP irradiated with diagnostic x-ray unit.....	62
Table 4.4	Dose sensitivity and correlation coefficient for different concentration of HEMA doped with 50 nm AuNP irradiated with diagnostic x-ray unit.....	64
Table 4.5	Dose sensitivity and correlation coefficient for different concentration of HEMA doped with 80 nm AuNP irradiated with diagnostic x-ray unit.....	66
Table 4.6	Dose sensitivity and correlation coefficient for different size of AuNPs for 5% of HEMA concentration irradiated with diagnostic x-ray unit.....	68

Table 4.7	Dose sensitivity and correlation coefficient for different size of AuNPs for 6% of HEMA concentration irradiated with diagnostic x-ray unit.....	70
Table 4.8	Dose sensitivity and correlation coefficient for different size of AuNPs for 7% of HEMA concentration irradiated with diagnostic x-ray unit.....	72
Table 4.9	Dose sensitivity and correlation coefficient for different size of AuNPs for 8% of HEMA concentration irradiated with diagnostic x-ray unit.....	74
Table 4.10	Dose sensitivity and correlation coefficient for different size of AuNPs for 9% of HEMA concentration irradiated with diagnostic x-ray unit.....	75
Table 4.11	Dose sensitivity and correlation coefficient for different concentration of HEA with no AuNP irradiated with diagnostic x-ray unit.....	87
Table 4.12	Dose sensitivity and correlation coefficient for different concentration of HEA doped with with 15 nm AuNP irradiated with diagnostic x-ray unit.....	89
Table 4.13	Dose sensitivity and correlation coefficient for different concentration of HEA doped with with 20 nm AuNP irradiated with diagnostic x-ray unit.....	91
Table 4.14	Dose sensitivity and correlation coefficient for different concentration of HEA doped with with 50 nm AuNP irradiated with diagnostic x-ray unit.....	93
Table 4.15	Dose sensitivity and correlation coefficient for different concentration of HEA doped with with 80 nm AuNP irradiated with diagnostic x-ray unit.....	95
Table 4.16	Dose sensitivity and correlation coefficient for different size AuNPs for HEA irradiated with diagnostic x-ray unit.....	97

LIST OF FIGURES

		Page
Figure 2.1	Diagram of an x-ray tube (Image from https://radiologykey.com/the-x-ray-tube-2/)	6
Figure 2.2	Illustration of Bremsstrahlung production.	7
Figure 2.3	Schematic illustration of spatial distribution of x-rays of different energy around a thin target.....	8
Figure 2.4	Illustration of the characteristic x-rays production	9
Figure 2.5	Illustration of Rayleigh (coherent) scattering.	11
Figure 2.6	Illustration of photoelectric effect.....	12
Figure 2.7	Illustration of the Compton Effect (Gibbons, 2020).....	13
Figure 2.8	Illustration of the pair production (Gibbons, 2020).....	13
Figure 2.9	Illustration of linear attenuation and x-ray transmission through absorber (Gunderson and Tepper, 2012a).....	14
Figure 2.10	Schematic of uv-vis spectrophotometer.....	16
Figure 2.11	The elimination of oxygen by ascorbic acid	24
Figure 2.12	the chemical structure of the monomer acrylamide, cross-linker BIS-acrylamide and polyacrylamide (Baldock et al., 1998; Lepage et al., 2001c; Karlsson et al., 2007)	26
Figure 2.13	Glass tubes containing VIPAR-gels. Gel A: non-irradiated. Gel B: absorbed 8 Gy integrated dose. The light part of gel C absorbed 11 Gy integrated dose while the transparent part did not absorb any dose (Pappas et al., 1999).....	30
Figure 3.1	Example of 4ml cuvette used. The dimension is 12mm x 45mm.	36
Figure 3.2	Schematic of the 10cm x 10cm Perspex with slots carved to fit a 12mm x 45mm cuvette.....	40
Figure 3.3	Illustration of the arrangement of samples embedded in the specially designed Perspex with another piece of Perspex laid above them.....	40
Figure 3.4	Rearrangement of layout in Figure 3.3 with superflab bolus inserted to fill the air gap.	41

Figure 4.1	Molecular structure of (a) 2-hydroxyethyl acrylate (HEA); (b) N, N'-methylene-bisacrylamide (BIS); (c) Polyhydroxyethylacrylate (pHEA).....	42
Figure 4.2	UV-Vis representation of absorbance for HEMA doped with 15 nm AuNP at different photon energy using LINAC	43
Figure 4.3	UV-Vis representation of absorbance for HEMA doped with 20 nm AuNP at different photon energy using LINAC	45
Figure 4.4	UV-Vis representation of absorbance for HEMA doped with 20 nm AuNP at 40 Gy photon energy using LINAC for the region 500-545 nm.	43
Figure 4.5	UV-Vis representation of absorbance for HEMA doped with 40 nm AuNP at different photon energy using LINAC.	46
Figure 4.6	UV-Vis representation of absorbance for HEMA doped with 40 nm AuNP at 50 Gy photon energy using LINAC for the region 490-540 nm.	47
Figure 4.7	UV-Vis representation of absorbance for HEMA doped with 50 nm AuNP at different photon energy using LINAC.	48
Figure 4.8	UV-Vis representation of absorbance for HEMA doped with 50 nm AuNP at 40 Gy photon energy using LINAC for the region 490-540 nm.	49
Figure 4.9	UV-Vis representation of absorbance for HEMA doped with 80 nm AuNP at different photon energy using LINAC.	50
Figure 4.10	UV-Vis representation of absorbance for HEMA doped with 80 nm AuNP at 40 Gy photon energy using LINAC for the region 490-540 nm.	50
Figure 4.11	UV-Vis representation of absorbance for HEMA doped with different size of AuNPs irradiated with 10 Gy LINAC.	51
Figure 4.12	UV-Vis representation of absorbance for HEMA doped with different size of AuNPs irradiated with 20 Gy LINAC.	52
Figure 4.13	UV-Vis representation of absorbance for HEMA doped with different size of AuNPs irradiated with 30 Gy LINAC.	53
Figure 4.14	UV-Vis representation of absorbance for HEMA doped with different size of AuNPs irradiated with 40 Gy LINAC.	54

Figure 4.15	UV-Vis representation of absorbance for HEMA doped with different size of AuNPs irradiated with 40 Gy LINAC focusing in the region 490-540 nm.	54
Figure 4.16	UV-Vis representation of absorbance for HEMA doped with different sizes of AuNPs at 50 Gy of photon energy.	55
Figure 4.17	plot of relaxation rate R2 vs Dose for different AuNPs size using 9% of HEMA for samples irradiated with LINAC	57
Figure 4.18	Plot of dose sensitivity vs. AuNP size at 9% of HEMA concentration for samples dope with 15 nm AuNP.	58
Figure 4.19	transverse relaxation rate R2 as the function of dose for HEMA samples at different monomer concentrations doped with 15 nm AuNP when irradiated with diagnostic x-ray machine	59
Figure 4.20	Plot of dose sensitivity vs. HEMA concentration for samples dope with 15 nm AuNP.	59
Figure 4.21	Transverse relaxation rate R2 as the function of dose for HEMA samples at different monomer concentration doped with 20 nm AuNP when irradiated with diagnostic x-ray machine	61
Figure 4.22	Plot of dose sensitivity vs. HEMA concentration for samples dope with 20 nm AuNP.	61
Figure 4.23	transverse relaxation rate R2 as the function of dose for HEMA samples at different monomer concentration doped with 50 nm AuNP when irradiated with diagnostic x-ray machine	63
Figure 4.24	Plot of dose sensitivity vs. HEMA concentration for samples dope with 50 nm AuNps.	63
Figure 4.25	transverse relaxation rate R2 as the function of dose for HEMA samples at different monomer concentration doped with 80 nm AuNP when irradiated with diagnostic x-ray machine	65
Figure 4.26	Plot of dose sensitivity vs. HEMA concentration for samples dope with 80 nm AuNps.	65
Figure 4.27	transverse relaxation rate R2 as the function of dose for HEMA samples at different AuNPs size for 5% HEMA concentration when irradiated with diagnostic x-ray machine.....	67
Figure 4.28	Plot of dose sensitivity vs. AuNPs size for 5% of HEMA concentration.....	67

Figure 4.29	transverse relaxation rate R2 as the function of dose for HEMA samples at different AuNPs size for 6% HEMA concentration when irradiated with diagnostic x-ray machine.....	69
Figure 4.30	Plot of dose sensitivity vs. AuNPs size for 6% of HEMA concentration.....	69
Figure 4.31	transverse relaxation rate R2 as the function of dose for HEMA samples at different AuNPs size for 7% HEMA concentration when irradiated with diagnostic x-ray machine.....	71
Figure 4.32	Plot of dose sensitivity vs. AuNPs size for 7% of HEMA concentration.....	71
Figure 4.33	transverse relaxation rate R2 as the function of dose for HEMA samples at different AuNPs size for 8% HEMA concentration when irradiated with diagnostic x-ray machine.....	73
Figure 4.34	Plot of dose sensitivity vs. AuNPs size for 8% of HEMA concentration.....	73
Figure 4.35	transverse relaxation rate R2 as the function of dose for HEMA samples at different AuNPs size for 9% HEMA concentration when irradiated with diagnostic x-ray machine.....	74
Figure 4.36	Plot of dose sensitivity vs. AuNPs size for 9% of HEMA concentration.....	75
Figure 4.37	Molecular structure of (a) 2-hydroxyethyl acrylate (HEA); (b) <i>N, N'</i> -methylene-bisacrylamide (BIS); (c) Polyhydroxyethylacrylate (pHEA).....	76
Figure 4.38	Absorption spectrum of uv-vis for undoped 5% HEA irradiated with different diagnostic x-ray energy.	77
Figure 4.39	Absorption spectrum of uv-vis for undoped 5% HEA irradiated with different diagnostic x-ray energy focusing on the region of 341 nm.	78
Figure 4.40	Absorption spectrum of uv-vis for undoped 5% HEA irradiated with different diagnostic x-ray energy focusing on the region of 364 nm.	79
Figure 4.41	Absorption spectrum of uv-vis for 5% HEA irradiated with different diagnostic x-ray energy doped with 15nm of AuNp.....	80
Figure 4.42	Absorption spectrum of uv-vis for 5% HEA irradiated with different diagnostic x-ray energy doped with 15nm of AuNp focusing on the region of 340-341 nm.....	80

Figure 4.43	Absorption spectrum of uv-vis for 5% HEA irradiated with different diagnostic x-ray energy doped with 15nm of AuNp focusing on the region of 364 nm.	81
Figure 4.44	Absorption spectrum of uv-vis for 5% HEA irradiated with different diagnostic x-ray energy doped with 20 nm of AuNp.....	82
Figure 4.45	Absorption spectrum of uv-vis for 5% HEA irradiated with different diagnostic x-ray energy doped with 20 nm of AuNp focusing on the region of 341 nm.	82
Figure 4.46	Absorption spectrum of uv-vis for 5% HEA irradiated with different diagnostic x-ray energy doped with 20 nm of AuNp focusing on the region of 364 nm.	83
Figure 4.47	Absorption spectrum of uv-vis for 5% HEA irradiated with different diagnostic x-ray energy doped with 50 nm of AuNp.....	84
Figure 4.48	Absorption spectrum of uv-vis for 5% HEA irradiated with different diagnostic x-ray energy doped with 50 nm of AuNp focusing on the region of 341 nm.	84
Figure 4.49	Absorption spectrum of uv-vis for 5% HEA irradiated with different diagnostic x-ray energy doped with 50 nm of AuNp focusing on the region of 364 nm.	85
Figure 4.50	the plot of R2 as a function of Dose for different concentration of HEA with no AuNP irradiated with diagnostic x-ray unit.....	86
Figure 4.51	Figure R2-dose sensitivity of different HEA concentration with no AuNP irradiated with diagnostic x-ray unit.....	87
Figure 4.52	the plot of R2 as a function of Dose for different concentration of HEA doped with 15 nm AuNP irradiated with diagnostic x-ray unit.....	88
Figure 4.53	R2-dose sensitivity of different HEA concentration doped with 15 nm AuNP irradiated with diagnostic x-ray unit.....	88

LIST OF ABBREVIATIONS

1D	One dimensional
2D	Two dimensional
3D	Three dimensional
3D–CRT	Three dimensional conformal radiotherapy treatments
AD	Analogue to Digital
ART	Algebraic reconstruction technique
AuNPs	Gold nanoparticles
BANANA	Bis, acrylamide, nitrous oxide and agarose dos
BANG	Bis, acrylamide, nitrogen and aqueous gelatin dosimeter
bis	N,N'-methylene-bis-acrylamide
CT	Computerized Tomography
DEF	Dose enhancement factor
Dmax	Maximum absorbed dose
dmax	Depth of maximum dose
FOV	Field of view
G	Gelatin
Gl	Glucose
GP	Genipin
Gy	Gray
H ₂ SO ₄	Sulfuric acid
IC	Ionizations chamber
ICRP	International Commission on Radiological Protection
IMRT	Intensity-modulated radiation therapy
IR	Ionizations radiation
keV	Kilo electron Voltage

LET	Linear energy transfer
LINAC	Linear accelerator
MAA	Methacrylic acid
MAG	Methacrylic Acid based Gel
MAGAS	Methacrylic acid, ascorbic acid, gelatin
MAGAT	Methacrylic acid, Gelatine And Tetrakis
MAGIC	Methacrylic , ascorbic acid in gelatin initiated by copper
MCA	Multichannel Analyzer
MRI	Magnetic Resonance Imaging
MU	Monitor unit
MV	Mega-voltage
NMAG	Normoxic Methacrylic acid based Gel
NMR	Nuclear Magnetic Resonance
NPAG	Normoxic Polyacrylamide Gel
OCT	Optical Computerized Tomography
OD	Optical density
PAG	Polymer acrylamide gel
PAGAS	Polyacrylamide Gel with Ascorbic acid
PAGAT	Polyacrylamide Gel And THPC
THPC	Tetrakis (hydroxymethyl) phosphonium chloride

PEMBANGUNAN DAN PENCIRIAN DOSIMETER GEL POLIMER TERDOP DENGAN PARTIKEL NANO EMAS

ABSTRAK

Kajian ini dijalankan menggunakan dua jenis monomer iaitu 2-Hydroxyethyl Acrylate (HEA) dan 2-Hydroxyethyl Methacrylate (HEMA) manakala N,N'-Methylene-bisacrylamide (BIS) sebagai pematik silang. Penghasilan sampel dilakukan secara 'normoxic' di bawah keadaan atmosfera biasa yang mana Asid Askorbik digunakan sebagai anti oksidan. Seperti kajian-kajian yang banyak dilakukan sebelum ini, kajian ini juga menggunakan sumber tenaga sinaran X yang tinggi iaitu pemecut linear (LINAC) dan mesin diagnostik sinar X sebagai suatu sumber tenaga radiasi utama. Bagi mengkaji kepekaan dos, ciri penyerakan dos di dalam gel polimer diperhatikan. Pengimejan Resonans Magnetik (MRI) adalah instrumen bacaan pengimejan utama yang dipilih dan imej yang diperolehi digunakan dalam pegiraan kepekaan dos. Bacaan data ini disokong dengan bacaan dari spektrofotometer UV-Visible. Secara amnya, kepekaan dos adalah berkadar langsung dengan kepekatan monomer, jumlah sinaran tenaga dan size partikel nano emas (AUNPs). Selain daripada partikel nano emas bersize 50 nm, sampel yang diberikan dos 30Gy menunjukkan tren penurunan serapan cahaya pada panjang gelombang melebihi 500nm. Tren penurunan adalah melebihi 10Gy dan 20Gy. Hasil kajian menunjukkan sampel yang diberikan sinaran x rendah, iaitu dari mesin diagnosis sinaran x, saiz nano emas dilihat memberi kesan berbanding sinaran x tinggi (pemecut linear). Pada tenaga X yang rendah, kepekatan monomer tidak terlalu memberi kesan terhadap proses pempolimeran. Pada tenaga X yang tinggi, sampel didopkan dengan AUNPs bersaiz 80nm menunjukkan kepekaan dos tertinggi. Kajian ini mendapati HEMA dan HEA

sangat sesuai dipasangkan dengan AuNP untuk dijadikan dosimeter. Kajian di masa hadapan boleh dilakukan dengan menggunakan jenis monomer yang berbeza, sumber tenaga alternatif dan pembolehubah lain yang sesuai.

DEVELOPMENT AND CHARACTERIZATION OF POLYMER GEL DOSIMETER DOPED WITH GOLD NANOPARTICLES

ABSTRACT

This study makes use of the advantage of normoxic polymer gels which are composed of two different monomer, 2-Hydroxyethyl Acrylate (HEA) and 2-Hydroxyethyl Methacrylate (HEMA) and N,N'-Methylene-bisacrylamide (BIS) as the crosslinker. To enable the fabrication of polymer gel to be done under the normal atmospheric condition, Ascorbic Acid is added as the anti-oxidant. As past studies had mainly been done using high energy sources, this study also focuses on using high energy x-ray source as in linear accelerator (LINAC) as well as a diagnostic x-ray unit as the main energy source. Dose sensitivity is property investigated in studying the behavior of dose distribution in the polymer gel. Magnetic Resonance Imaging (MRI) is the main polymerization imaging readout instrument before the images are used for further calculation of dose sensitivity. The results obtained are backed up by the analysis using UV-Visible spectrophotometer. In general, the dose sensitivity is directly proportional to the irradiation energy, monomer concentration and AuNPs size. When HEMA is used as the monomer, higher irradiation dose by LINAC increases the absorption of light. This is true for all the size of AuNPs used in this study (15nm, 20 nm, 40nm, 50nm and 80nm). Except for 50nm AuNP size, samples irradiated with dose of 30Gy shows a decreasing absorption of light at wavelength over 500nm. The decreasing pattern goes below than the samples irradiated with 10Gy and 20Gy. The result shows that at low x-ray energy, the size of AuNP has an impact on the polymerization. Higher concentration of monomer does not affect the polymerization significantly at the low energy level. At high x-ray energy, AuNPs of

80 nm in size has the highest dose sensitivity. The significance of this study can benefit in the cancer treatment planning and the treatment itself. Further studies could be done using different types of monomers, alternative energy sources and other possible variables.

CHAPTER 1

INTRODUCTION

1.1 Background

Cancer remains as one of the highest causes of death with patients diagnosed with cancer are rapidly increasing in numbers. In 2018, 18.1 million new cancer cases were reported and it is expected to reach 27 million cases per year in 2040 (Wild et al., 2020). The 50% increase is undoubtedly worrying especially in countries with low Human Development Index (HDI). This is due to the under-equipped hospitals and the limited accessibility to those in need.

Rapid increase in number of cancer cases calls for the best treatment available. Surgery, chemotherapy and radiotherapy are the main approaches used in treating cancer. These approaches are delivered separately or combined (Sánchez-Santos 2012). Surgery and radiotherapy are the primary methods for treating non metastatic tumours, while for patients with metastatic cancer, chemotherapy is usually applied as combined treatment (Haume et al., 2016). Metastatic is defined as spread of cancerous cells to other parts of body from where it originated and vice versa.

For this study, the author will focus on radiotherapy using Intensity Modulated Radiation Therapy (IMRT) and to be compared with the diagnostic x-rays. As a major treatment approach, radiotherapy needs a near perfect pre-treatment planning. The said planning is to locate the exact location of the cancerous cells and the dose needed for irradiation. This crucial step is not only to eliminate the tumor, but also keep healthy cells from unneeded irradiation.

The accidental discovery of x-rays in late 19th century has since proven its importance in medical world. The discovery of the biological effect of x-rays followed a couple of years after x-rays discovery. It is known that x-ray is one of the ionizing radiations which can fatally effect human. This property of x-rays has been taken advantage of and be utilized clinically in cancer treatment. While ionizing radiation is an essential tool to eliminate cancerous cells, it needs to be handled cautiously to avoid its interaction with the healthy cells. With the increasing numbers of therapeutic techniques, it is highly essential to have an effective delivery method. For this reason, treatment planning is done before proceeding with the irradiation treatment. Over the years, the precision of dose delivery toward the cancerous cells has improved while minimizing the unwanted absorption of the dose by the healthy cell.

The technique involved in measuring the absorbed dose is called dosimetry. Among the most commonly used dosimeter are thermoluminescent dosimeter (TLD), Geiger tube, personal dosimeter and etc. Dosimeters can be used in calibration of radiation related instruments and they are widely used to monitor the delivered dose to patients. In maximizing the absorbed dose by the target while avoiding the absorption by the healthy dose, the measurement of absorbed dose is very important. Thus, the dose measurement is developed as the fundamental of this study.

Radiotherapy has become one of the most widely applied technique in treating cancer. In 2016, there were an estimated of 10.5 million cancer survivors in The United States of America. 3.05 million of them have the history of receiving radiotherapy treatment. (Bryant et al., 2017). With 29% of the survivors receiving radiation related treatment, the ability of radiotherapy has proven to be crucial in the

medical field. Since the discovery of biological effect of radiation towards human, extensive studies have been made in utilize this advantage in treating cancer. One of the most important developments is the medical linear accelerator (LINAC) which use high energy x-rays as the source of radiation. LINAC does not only produce high x-ray energy in killing the tumor but improves the targeting ability in minimizing the effect to the healthy cells.

1.2 Problem Statement

High number of cancer related cases causes attracted many studies in the field (Haume et. al., 2016; Rosa et. al., 2017; Mokoena et. al., 2019). The difficult and complex task of delivering the radiation needed towards the tumor in radiation therapy needs extra cautious in the process. This is due to the possibility of the deposited energy negatively affecting the healthy tissues (Haume et al., 2016). To reduce the unwanted radiation on the healthy cell, an excellent dosimetry system is needed. This includes to find the dose distribution of the radiation. Polymer gel dosimeter has become one of the most used tools in determining 3D dose distribution (Sam-Joo et. al., 2010; Venning et. al., 2005b). The early days polymer gels are highly sensitive toward oxygen that led polymerization. Instead of using the old ways of utilizing glove box while preparing the gel dosimeter, the samples in this study are manufactured with anti-oxidant that chemically discard oxygen from interacting with them (Sam-Joo et. al., 2010). Two types of monomers are used in this study, namely 2-Hydroxyethyl methacrylate (HEMA) and 2-hydroxyethyl acrylate (HEA) with co-monomer. N,N'-Methylene-bisacrylamide (BIS). BIS is functioning as the crosslinker which helps the monomers to link to each other does increases the rate of polymerization.

This study focuses on the effect of the concentration of the monomers and the size of AuNPs. Since radiation therapy such as LINAC uses extremely high photon energy, it is necessary to find a dose enhancer in minimizing the dose given. AuNP is seen to be one of the best additions in polymer gel dosimeter in enhancing the radiation dose. This is due to its high atomic number ($Z=79$) and mass coefficient relative to soft tissue (Rosa et. al., 2017). The high mass energy coefficient (100-150 times higher) means the probability of photoelectric interaction also increases thus resulting in deposition of energy at the target (Hubbell and Seltzer 1996). This theory is the basis of investigating the possibility of AuNP as a dose enhancer. Dose sensitivity and absorbance will be the main indicator in determining the effect of AuNP towards polymerization.

1.3 Objectives

The objectives of this study are:

1. To develop two different polymer gel dosimeters, namely 2-Hydroxyethyl methacrylate (HEMA) and 2-hydroxyethyl acrylate (HEA) with co-monomer. N,N'-Methylene-bisacrylamide (BIS). Polymer gel dosimeter has to solid enough to record the 3D dose distribution of the radiation.
2. To evaluate the effect of monomer concentration towards polymerization. This is to find the best monomer to be used as dosimeter and be paired with suitable AuNPs.
3. To investigate the effect of presence of AuNP towards polymerization. Along with that, the effect of the AuNPs size will also be evaluate.

1.4 Scope of study

This study covers the field of dose distribution which is measured using gel dosimeters. For this purpose, 2-Hydroxyethyl methacrylate (HEMA) and 2-hydroxyethyl acrylate (HEA) are used. This is to see the effect of dose distribution in different polymers. AuNP of different sizes are used to investigate its effect along with the monomer concentration. The limitation regarding the samples preparation and irradiation are the unavailability of other common monomers such as acrylamide and methacrylamide and other source of data analysis such Raman spectroscopy.

Other variables that are excluded from this study are such the effect of depth of gel dosimeters in a phantom, the effect of BIS concentration and the effect of anti-oxidant concentration.

1.5 Thesis outline

Chapter one will be a brief introduction about this study. The surface of the theory and literature review will be written briefly. Chapter two will be discussing the theory involved behind related to this study. Details on literatures used as references will also be discussed in details in this chapter. It will provide a little more understanding on the direction of this study. Chapter three is the details on materials used in this study, including the preparation of the polymer gel until the analyzing process. In Chapter four, all the findings will be presented and discussed in details. And this thesis will be concluded in Chapter five together with suggestion of future study.

CHAPTER 2 THEORY AND LITERATURE REVIEW

2.1 Discovery of x-ray

In 1895, Roentgen was studying the cathode rays in a gas discharge tube. He accidentally discovered a new type of radiation formed outside of the tube, which he presumed due to the interaction of electrons with the glass tube. This new radiation was found to have the ability of penetrating the opaque bodies, produce fluorescence, blacken a photographic plate and ionize gas. This unique radiation was named x-ray simply for its namelessness.

2.2 Production of x-ray

Figure 2.1 is a diagram of an x-ray tube. In an x-ray tube, a cathode is fixed at one end and an anode the other end. Both of the electrodes are hermetically sealed. A high voltage between anode and cathode causes the heating of the filament. Thermionic emission occurs when the tungsten filament of the cathode emits electrons due to the heating. These electrons will move with very high velocity towards the tungsten target placed at the anode. The sudden stoppage of the electrons movement will cause the loss of energy in the form of x-ray. The x-ray beam produced is directed towards the port or also known as window (Gibbons, 2020).

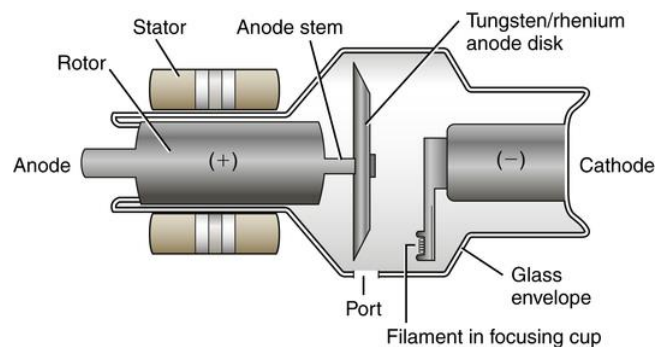


Figure 2.1 Parts of the x-ray tube. A cross-sectional view of a basic rotating anode x-ray tube. (Radiology Key, 2016).

2.3 Types of x-rays

2.3.1 Bremsstrahlung

There are two types of x-ray produced by the x-ray tube namely Bremsstrahlung and characteristic x-ray. Bremsstrahlung is a German word translated as braking radiation. This phenomenon occurs when an accelerating electron passes near a nucleus and the path of the electron gets deflected due to force of attraction. During the change of its path, the electron loses certain amount of energy known as Bremsstrahlung where it can propagate through the space as electromagnetic radiation. An electron may lose a part or all of its energy during the interaction with the nucleus resulting in the ability of Bremsstrahlung photon released to have the maximum energy of the initial electron. The illustrated mechanism of Bremsstrahlung production is shown in Figure 2.2.

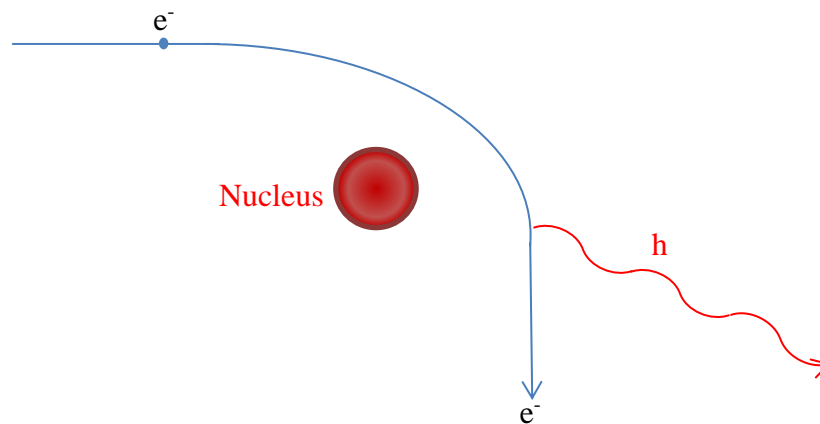


Figure 2.2 Illustration of Bremsstrahlung production.

The direction of the Bremsstrahlung photons is determined by the energy of the incident electron. When the energy of the incident electrons is less than 100keV, the emitted x-rays are equal in all directions. By referring Figure 2.3, it is seen that as the kinetic of the incident electrons increases, the direction of the x-rays produced

becomes increasingly forward. At low electron energy, the x-ray beam is obtained 90° from the incidence of electrons while at high electron energy the x-ray beam is produced on the other side of incident electrons.

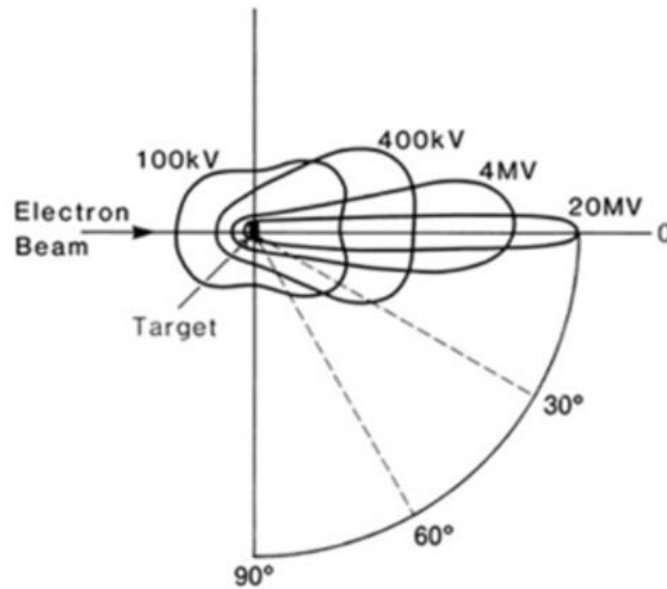


Figure 2.3 Schematic illustration of spatial distribution of x-rays of different energy around a thin target

2.3.2 Characteristic x-ray

When an incident electron accelerates towards a target, it may interact with the atoms of the target. Upon colliding with an atom, the electron may eject an orbital electron usually K, L or M electron. With carrying energy of E_0 , the incident electron has the ability to eject the orbital electron while giving ΔE energy, resulting in the receding of the former with energy of $E_0 - \Delta E$. A part of ΔE is consumed to overcome the binding energy, EB_K (Figure 2.4) of the K orbital electron and the rest is carried by the electron during ejection.

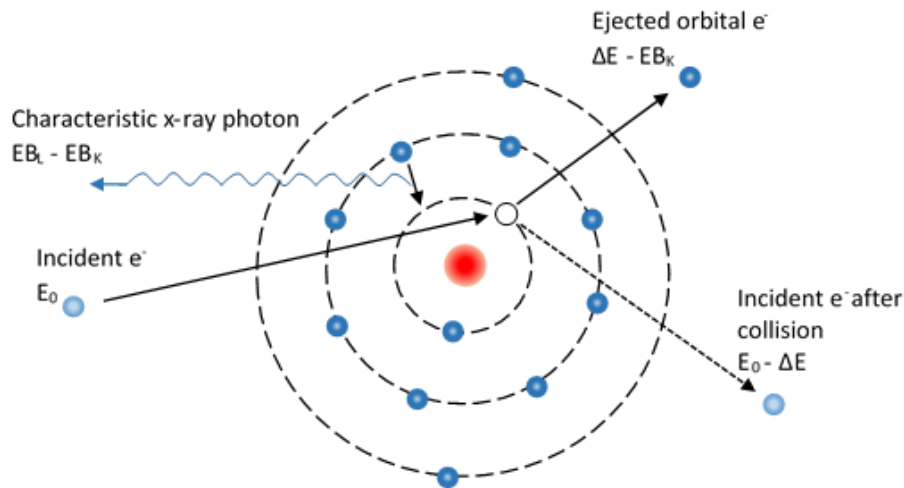


Figure 2.4 Illustration of the characteristic x-rays production

The space left by the ejected electron results in falling of an electron from the outer orbit to occupy the vacancy. The orbital transition by the electron leads to the release of energy in the form of electromagnetic radiation carrying the energy of $EB_L - EB_K$. This radiation is known as the characteristic radiation.

The energy of the radiation depends on the element of the target, where it carries the characteristic of the target, hence the name characteristic radiation. Targets with high atomic (Z) number and most inner shells such as K and L involved in the transition of electron, are able to emit the characteristic radiation high enough to be considered as x-rays. Table 2.1 shows the major characteristic radiation energies produced in a tungsten target.

Table 2.1 Principal characteristic x-ray energies for Tungsten (Radiological Health Handbook Revised Edition, 1970)

Series	Lines	Transition	Energy (keV)
K	$K\beta_2$	$N_{III}-K$	69.09
	$K\beta_1$	$M_{III}-K$	67.23
	$K\alpha_1$	$L_{III}-K$	59.31
	$K\alpha_2$	$L_{II}-K$	57.97
L	$L\gamma_1$	$N_{IV}-L_{III}$	11.28
	$L\beta_2$	N_V-L_{III}	9.96
	$L\beta_1$	$M_{IV}-L_{II}$	9.67
	$L\alpha_1$	M_V-L_{III}	8.40
	$L\alpha_2$	$M_{IV}-L_{III}$	8.33

2.4 Interaction of photons with matter

Series of successful x-ray beam production Attenuation of photon beam occurs through four major interactions namely Rayleigh (coherent) scattering, photoelectric effect, Compton scattering and pair production.

2.4.1 Rayleigh scattering

As an electromagnetic wave passing through near an electron, it may cause the oscillation of the electron. Rayleigh scattering is the phenomenon when the oscillating electron release the energy received at the exact wavelength as the incident wave (Figure 2.5). The change is only in the scattering of the photons at a small angle but none towards the wave form.

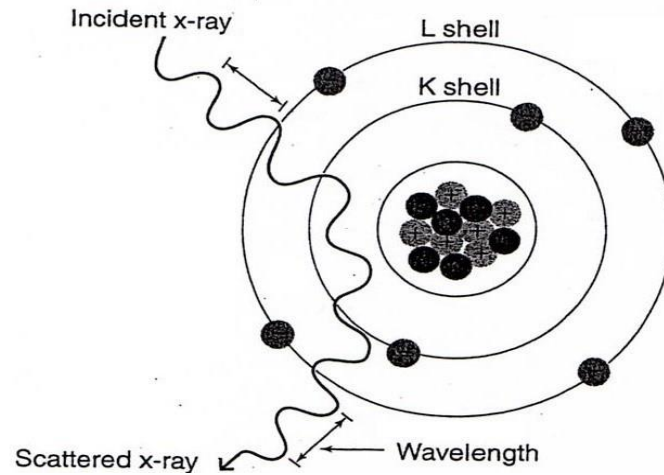


Figure 2.5 Illustration of Rayleigh (coherent) scattering.

2.4.2 Photoelectric effect

Upon interaction with an atom, energy of photons can be transferred to an inner electron causing the electron to be ejected from the orbit leaving an empty spot on the involved orbit. The ejected electron which is known as the photoelectron has the energy of $h\nu - E_B$, where $h\nu$ is the energy of the incident x-rays and E_B is the binding energy of the electron. The vacancy left by the photoelectron can be filled by an outer orbital electron while emitting characteristic x-ray. Another possibility is the emission of the Auger electrons which occur when the energy release by the outer shell electron in the process of filling the vacant shell is absorbed by another outer shell electron. This will excite the electron thus ejected from the shell as Auger electron (Figure 2.6).

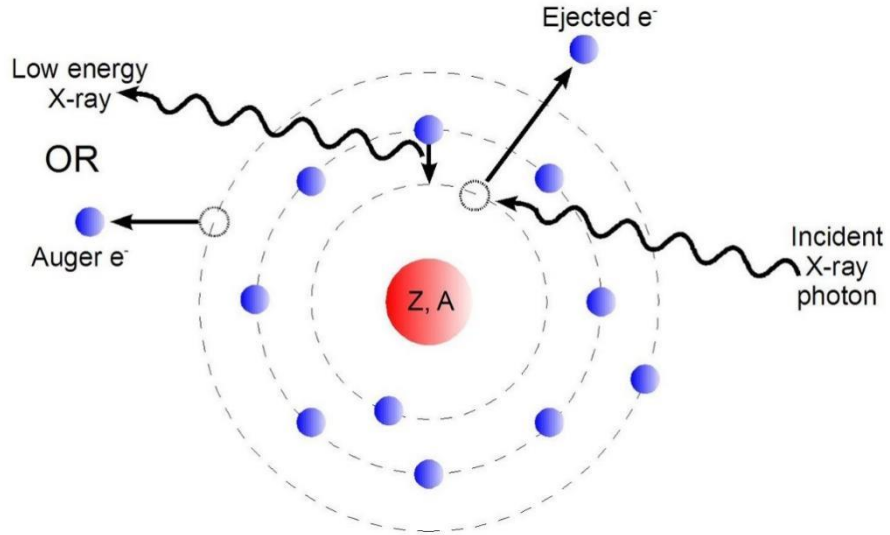


Figure 2.6 Illustration of photoelectric effect.

2.4.3 Compton Effect

When incident photon of $h\nu_0$ energy collides with an atomic electron with a very low bonding energy, the energy absorbed by the electron might cause the electron to be ejected at an angle θ . The photon will be diverted at an angle ϕ with reduced energy (Figure 2.7). Equation 2.1, 2.2 and 2.3 shows the relationships of the said energies by following the laws of conservation of energy and momentum:

$$E = h\nu_0 \frac{\alpha(1-\cos\phi)}{1+\alpha(1-\cos\phi)} \quad 2.1$$

$$h\nu' = h\nu_0 \frac{1}{1+\alpha(1-\cos\phi)} \quad 2.2$$

$$\cot\theta = (1 + \alpha)\tan\phi/2 \quad 2.3$$

Where $h\nu_0$, $h\nu'$, and E are the energies of incident photon, diverted photon and ejected electron respectively. $\alpha = h\nu_0/m_0c^2$ where m_0c^2 is the rest energy of the electron (0.511MeV). Thus in term of MeV, $\alpha = h\nu_0/0.511$.

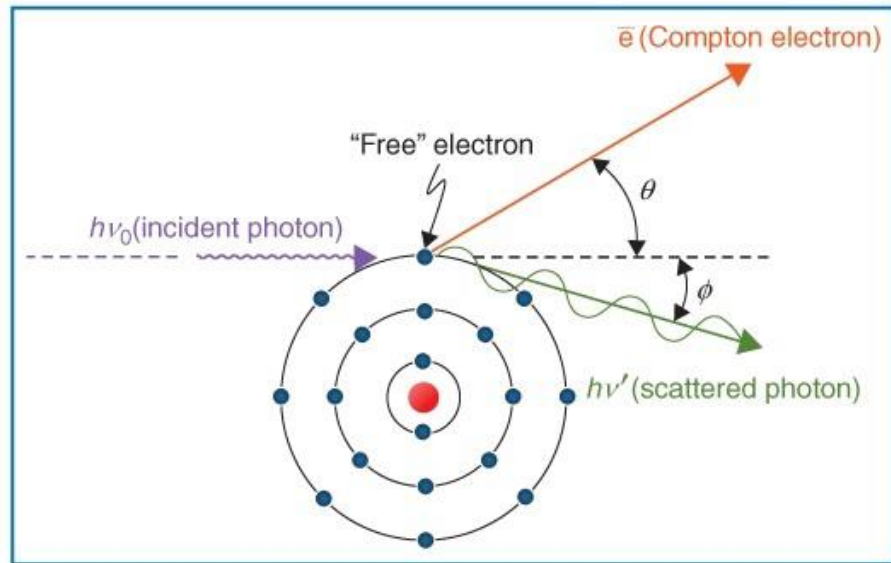


Figure 2.7 Illustration of the Compton Effect (Gibbons, 2020)

2.4.4 Pair Production

Pair production is the interaction of incident photon with energy greater than 1.02 MeV with the electromagnetic field of a nucleus (Figure 2.8). The photon ends up losing all of its energy to produce pair of negative electron (e^-) and positive electron (e^+) or better known as positron. The rest mass of the electron is 0.51 MeV, thus to produce two electrons in a pair production process, a minimum energy of 1.02 MeV is required. The electron-positron pair has the total kinetic energy of $(h\nu - 1.02 \text{ MeV})$ with the direction of the pair is in forward direction relative to the incident photon.

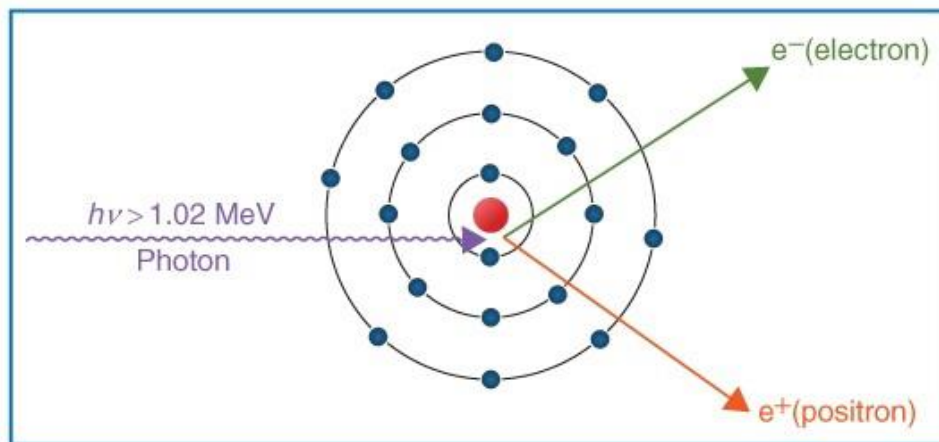


Figure 2.8 Illustration of the pair production (Gibbons, 2020)

2.5 The Attenuation of X-ray

A successful production of x-ray will be directed to an object, a patient in case of diagnostic x-ray unit, and can be completely absorbed or scattered from its initial path. The scattered photons loses some of their energy while some pass through the object without going any interaction. The interactions occurred between the photons and the object cause photons to be depleted in numbers and this phenomenon is called the attenuation of x-ray.

2.5.1 Linear Attenuation Coefficient

The intensity of a beam of monoenergetic photons decreases due to its interactions with the material passing through the attenuator. The reduction in the intensity is mainly determined by the thickness, density and atomic number of the attenuator (Powsner et al., 2013, Seegenschmiedt et al., 2009). The illustration of linear attenuation coefficient (μ) according the penetration and intensity reduction of the incident photons beam through an attenuator is in Figure 2.9.

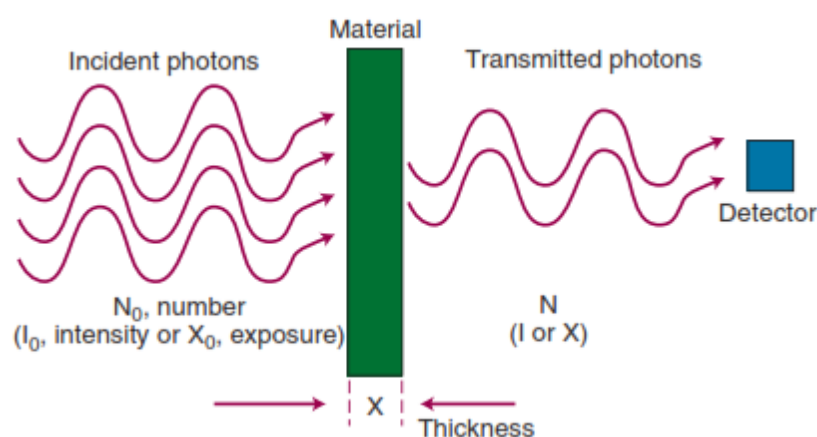


Figure 2.9 Illustration of linear attenuation and x-ray transmission through absorber (Gunderson and Tepper, 2012a)

2.6 Linear Accelerator (LINAC)

Most external beam therapy is performed using photon beams. These beams are used to treat cancer by targeting the tumor cells. One of the most utilized high-energy x-ray radiation is called use linear accelerator (LINAC) which has the ability to produce a beam of electrons or X-rays (Podgorsak, 2005b). A quality control program should be carried out when comparing the results of treatment plans against the experimental data. The data should be collected using dosimetric parameters such as the dose profile and the depth of the beam. Before a dose is delivered, it is important to determine the dosimetric parameters of the photon beam to achieve a dose distribution that is consistent with the target volume. The percentage depth-dose data is very important for assessing the patient's dose during diagnostic x-rays (Ramirez et al., 2012). In contrast, the quality of a radiation beam is measured in terms of its penetrating power.

2.7 UV-Visible spectrophotometer

Explanation of UV-Visible spectrometer theory is from Barron *et al* (2011) as illustrated in Figure 2.10. Uv-vis spectrophotometer has the coverage of light ranging from 200 nm to 800 nm. Since this range of light can never be achieved by single light source, a deuterium lamp and tungsten or halogen lamp are usually paired together. The former is to provide light in the ultraviolet range and both of the latter to achieve the visible part. The lamp emits light towards the diffraction grating where it separates the light according to their respective wavelength before reaching the slit.

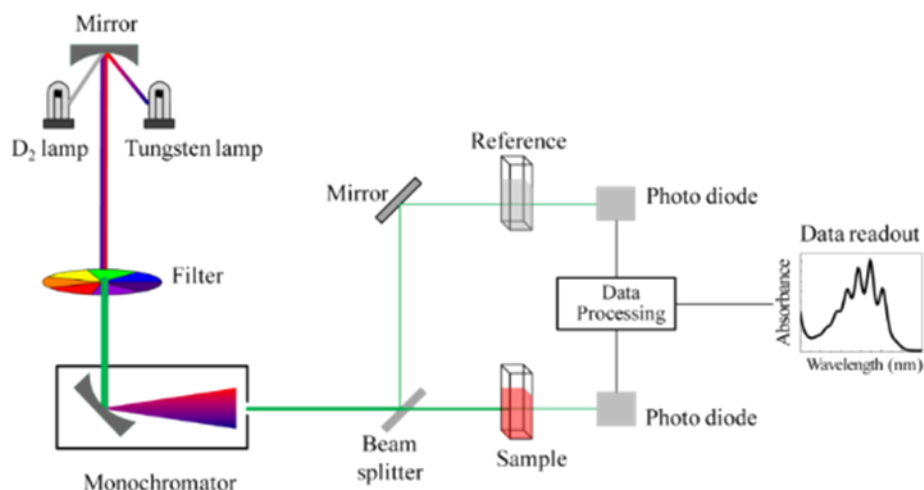


Figure 2.10 Schematic of uv-vis spectrophotometer.

Upon reaching the slit, the light will pass through the sample, mirror and the rotating disc where it is next directed towards the detector. The detector role is to convert the signal collected from light form to a current signal. The current will then be submitted to uv-vis spectrophotometer computer system to lay out the result such as absorbance. Absorbance, A , is calculated by using Equation 2.4:

$$A = \log_{10} \frac{I_0}{I} \quad 2.4$$

I is the sample cell intensity and I_0 is the reference cell intensity.

The following cases are possible:

Where $I > I_0$ and $A < 0$. This mostly occurs when using the unsuitable solvent where the solvent used absorbs light in the wavelength range. To obtain an accurate reading, solvent should be changed.

Where $I = I_0$ and $A = 0$. This occurs when both reference and sample cells are filled with pure solvent. This is the best test to be done before the actual reading is taken to ensure the cleanliness of the cuvette used.

When $A = 1$. When the light is being absorb at 90%, this means only 10% of light are being allowed to be detected. So I_0/I becomes $100/10 = 10$ or $I=0.1I_0$.

When $A > 1$. This is an extreme condition where light is absorbed more than 90%. The saturated compound of the sample used could be one of the reason.

2.7.1 Effect of concentration and container shape on absorbance

The light emitted from the source will pass through the samples. The capability of the sample to absorb light depends on many factors, in this study the polymerization of monomer plays the main role in determining the absorbance. The more cross-linking of monomer and co-monomer occur, the closer polymer chain are formed to each other. Close knit chain prevents more light from passing through thus results in higher absorbance.

When two exact same samples are put in containers with same shape but of different size, the absorbance value will definitely be different. The light travelling through a sample in 1 cm container would have a shorter travelling time compared to light passing through a 10 cm container. Short travelling time give less interaction time thus will result in lower absorbance

2.7.2 Beer-Lambert Law

The Beer-Lambert law explains the relationship between the distant travelled by light and concentration of a sample with absorbance (Equation 2.5 & 2.6).

$$\log_{10} \frac{I_0}{I} = \epsilon lc$$

2.5

As mentioned before, absorbance, $A = \log_{10} \frac{I_0}{I}$ so the above equation can be simplified as:

$$A = \epsilon lc$$

2.6

where ϵ is the molar absorptivity or molar absorption coefficient; l is the path length of light in cm; and c is the concentration of solution.

2.8 Polymer gel dosimetry

2.8.1 Fricke gel dosimeters

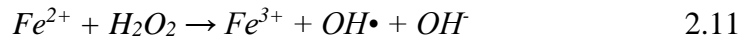
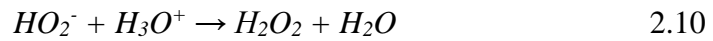
Early days polymer gel used as dosimeter is called the Fricke gel dosimeter which is named after the inventor itself. Acting as a single point dosimeter, Fricke dosimeter is fabricated using ferrous sulphate, FeSO_4 solution (Fricke and Morse, 1927). In 1984, a proposal of stabilizing the geometric dose information by combining the Fricke solution into gel matrix (Gore et al., 1984). Together with this new development, magnetic resonance imaging (MRI) is further used in obtaining the spatial dose distribution in three dimension. Fricke gel is the foundation of modern polymer gels development.

Dose dependant transformation of ferrous ions (Fe^{2+}) to ferric ions (Fe^{3+}) is the dosimetric basis in Fricke dosimeter. The process started upon irradiation of the

solution, where water decomposition takes place. Hydrogen atoms produced react with oxygen to produce hydroperoxy radical (Equation 2.7).



Equation 2.8-2.11 shows the subsequent reactions following the decomposition of water lead to the conversion of Fe^{2+} to Fe^{3+} .



The number of Fe^{3+} produced is dependent on the energy absorbed by the Fricke solution. The change in Fe^{3+} follows Equation 2.12:

$$\Delta[Fe^{3+}] = \frac{D \cdot G(Fe^{3+}) \cdot 10\rho}{N_A \cdot e} \quad 2.12$$

where D is the dose, $G(Fe^{3+})$ is the chemical yield of Fe^{3+} (expressed in ions produced per 100 eV), ρ is the density in kg liter⁻¹, N_A is Avogadro's number and e is the number of Joules per electron volt. The change in concentration of Fe^{3+} can be calculated and used in measuring the absorbed dose. This has become the basis of Fricke gel dosimetry.

The ferrous ions in Fricke gel are converted to ferric ions upon irradiation. The evaluation of the distribution of ferric ions can be done using MRI. The gel matrix helps in maintaining the spatial distribution of the ferric ions so that the spatial integrity of the dosimeter can be assured. Over the time, the ferric ions will start to diffuse thus affecting the distribution of ferric ions. Consequently, this will result in blurring of the MRI. This limitation leads to the finding of alternative

polymer gel which is developed using acrylic monomer solidified in gelatine or agarose matrix. It was found that this type polymer gel stabilizes the dose distribution post irradiation (Balcom et al., 1995; Baldock et al., 1995, 2001; Harris et al., 1996; Kron et al., 1997; Olsson et al., 1992b; Pedersen et al., 1997; Schulz et al., 1990; Maryanski et al., 1993).

2.8.2 Acrylic based polymer gel dosimeters

In 1993, Maryanski et. al. (1993) developed a new type of polymer gel dosimeters using acrylic as the monomer. Acrylamide is used as the monomer and N,N'-methylene-bis acrylamide (BIS) as a co-monomer which also act as the crosslinker in binding the polymer of acrylic upon interaction with ionizing radiation. The long chain of acrylic polymer fixed the Fe³⁺ diffusion problem in Fricke gel.

After the discovery of this new type of polymer gel, researchers have developed other type of polymer gel using various formulation. Among the polymer gels are BANANA (BIS-acrylamide, Acrylamide, Nitrous oxide and Agarose), BANG-1TM (BIS acrylamide, acrylamide, nitrogen, gelatin) (Maryanski et al., 1993, 1994), BANG-2TM (BIS acrylamide, acrylamide, sodium hydroxide, nitrogen, gelatin) (Maryanski et al., 1996), BANG-3TM (BIS acrylamide, methacrylic, sodium hydroxide, nitrogen, gelatin), PAG (polyacrylamide gel) (Baldock et al., 1998b), VIPAR (N-vinylpyrrolidone-argon based) (Kipouros et al., 2001), HEA (2-hydroxyethyle acrylate, bis-acrylamide acrylamide gelatin) (De Deene et al., 2002a).

Besides acrylamide as the monomers, there other polymer gels developed using different type of monomers namely acrylic acid (ACA), methacrylic acid

(MCA), 1-Vynil-2-pyrrolidinone (VP), 2-Hydroxyethyl acrylate (HEA), 2-Hydroxyethyl methacrylate (HEMA), acrylamide (AA) and methacrylamide (MAA).

The existence of oxygen is known to be one of the factor that can contaminate the polymer gel dosimeter. It is found that oxygen has the ability in initiating the polymerization and crosslinking process prior to irradiation (Hepworth et al., 1999a; Salomons et al., 2002). Therefore, in preparing such polymer gels, it is done in a nitrogen glove box where nitrogen gas is commonly passed through the polymer gels during fabrication. The nitrogen gas will displace oxygen hence avoiding the contamination of the prepared polymer gels. It is a very time-consuming process considering the difficult handling in the glove box and the time taken by the nitrogen gas in disposing the oxygen.

2.8.3 Normoxic polymer gel

The answer in overcoming the difficulties faced in preparing the polymer gel in a nitrogen glove box has finally answered in developing MAGIC polymer gels (Fong et al., 2001). This was when polymer gel dosimeter was successfully fabricated and irradiated in normal atmospheric condition. There was no nitrogen glove box used in eliminating the oxygen from polymer gels, instead an anti-oxidant was introduced in the polymer gels mixture. The addition of the anti-oxidant makes it possible for the polymer gels to be developed under normal atmosphere. Normoxic means normal oxygen level which symbolizes the normal atmospheric condition. There were several anti-oxidants put under investigation (De Denee et al., 2002a) but three of the best in eliminating oxygen are ascorbic acid, N-acetylcysteine and tetrakis(hydroxymethyl)phosphonium chloride (THPC). With the

newly found technique, several studies have been conducted using normoxic polymer gels. The summary is as in Table 2.2.

Table 2.2 Several polymer gel dosimeters manufactured under normoxic condition.

No	Reference	Polymer gel formulation and Acronym gel type	Concentrations (%)
1.	Fong <i>et al.</i> , 2001	Methacrylic acid <i>Ascorbic acid</i> <i>Hydroquinone</i> CuSO ₄ ·5H ₂ O Gelatine Deionized water MAGIC gel	9 0.0352 2 0.002 8 82.8
2.	Deene <i>et al.</i> , 2002a; 2002b	Methacrylic acid <i>Ascorbic acid</i> <i>Hydroquinone</i> CuSO ₄ ·5H ₂ O Gelatine Deionized water MAGIC gel	9 0.2 mM, 2mM 20 mM 0 – 10 mM 8 83
3.	Deene <i>et al.</i> , 2002a	Methacrylic acid <i>Ascorbic acid</i> Gelatine Deionized water MAGAS gel	9 5 mM 8 83
4.	Deene <i>et al.</i> , 2002a	Acrylamide <i>N,N</i> -methylene-bis-acrylamide <i>ascorbic acid</i> Gelatine Deionized water PAGAS gel	4.5 4.5 5 mM 8 83
5.	Deene <i>et al.</i> , 2002a	Methacrylic acid <i>Tetrakis (hydroxymethyl) phosphonium chloride</i> Gelatine Deionized water MAGAT gel	9 1 – 100 mM 8 83

6.	Brindha <i>et al.</i> , 2004b	Acrylamide <i>N,N</i> -methylene-bis-acrylamide <i>Tetrakis(hydroxymethyl) phosphonium chloride</i> Gelatine Deionized water PAGAT gel	3 3 0.19 5 89
7.	Brindha <i>et al.</i> , 2004b	Methacrylic acid <i>Tetrakis (hydroxymethyl) phosphonium chloride</i> Gelatine Deionized water MAGAT gel	9 0.19 8 83
8.	Hurley <i>et al.</i> , 2005	Methacrylic acid <i>Tetrakis (hydroxymethyl) phosphonium chloride</i> <i>Hydroquinone</i> Gelatine Deionized water MAGAT gel	9 1 -100 mM 0 – 50 mM 8 83
9.	Venning <i>et al.</i> , 2005a	Methacrylic acid <i>Ascorbic acid</i> Gelatine Deionized water MAGAS gel	9 5 mM 8 83

2.8.4 Ascorbic acid as anti-oxidant

As mentioned in Section 2.8.3, the addition of anti-oxidant is enough to eliminate the oxygen (De Denee *et al.*, 2002a; Venning *et al.*, 2005a). One of the best anti-oxidant to be used in polymer gel dosimeters is ascorbic acid. The property of the anti-oxidant that helps in displacing oxygen (Figure 2.11) is the ability to form a bond with the oxygen.

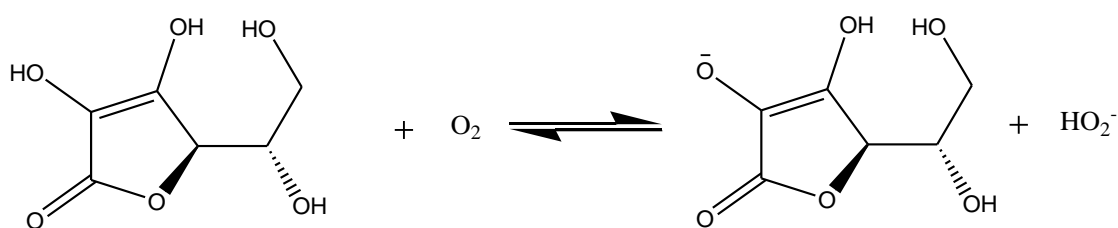


Figure 2.11 The elimination of oxygen by ascorbic acid

In terms of biological molecules, the four most abundant elements are hydrogen, nitrogen, carbon, and oxygen. Their atomic number helps determine the chemical bonds between them. It's known that having a certain number of electrons helps in maintaining a certain chemical bond. For instance, in ascorbic acid, the C-O-H bond can be broken by the presence of oxygen and water. Before the ascorbic acid is subjected to irradiation, the H^+ ion it will interact with O_2 and become HO_2^- . This process will increase the number of ions in the solution. Upon irradiation, HO_2^- ions interact with H^* to gradually transform into a hydrogen peroxide, H_2O_2 .

In order to maintain the covalent bond, the O^- in the ascorbic acid will be attracted to the hydrogen free radicals, RH . This process will not affect the process of producing the various components of a product.

2.8.5 Polymerization of Polymer Gel

Crosslinking and free-radical induced polymerization is a the four-step process involving free radical production, initiation, propagation and termination of polymer. The gel system is composed of 90% water by weight. The reaction to the absorbed dose is initiated by the radiochemical reaction of water. Free radicals are created through the radiolysis of water. They are then initiated with the formation of free units from a single monomer. The resulting free radicals are then added to the end of the chain through propagation reactions.